ChemPubSoc Europe
DOI: 10.1002/cssc.201901739
CHEMSUSCHEM Full Papers

Concentrated Ionic-Liquid-Based Electrolytes for High-Voltage Lithium Batteries with Improved Performance at Room Temperature

Xinpei Gao,[a, b] Fanglin Wu,[a, b] Alessandro Mariani,[a, b] and Stefano Passerini*[a, b]

Ionic liquids (ILs) have been widely explored as alternative electrolytes to combat the safety issues associated with conventional organic electrolytes. However, hindered by their relatively high viscosity, the electrochemical performances of IL-based cells are generally assessed at medium-to-high temperature and limited cycling rate. A suitable combination of alkoxy-functionalized cations with asymmetric imide anions can effectively lower the lattice energy and improve the fluidity of the IL material. The Li/$Li_{1.2}Ni_{0.2}Mn_{0.6}O_2$ cell employing *N*-*N*-diethyl-*N*-methyl-*N*-(2-methoxyethyl)ammonium (fluorosulfonyl)(trifluoromethanesulfonyl)imide (DEMEFTFSI)-based electrolyte delivered an initial capacity of 153 mAh g^{-1} within the voltage range of 2.5–4.6 V, with a capacity retention of 65.5% after 500 cycles and stable coulombic efficiencies exceeding 99.5%. Moreover, preliminary battery tests demonstrated that the drawbacks in terms of rate capability could be improved by using Li-concentrated IL-based electrolytes. The improved room-temperature rate performance of these electrolytes was likely owing to the formation of Li^+-containing aggregate species, changing the concentration-dependent Li-ion transport mechanism.

Introduction

Room-temperature ionic liquids (RTILs) offer a unique suite of properties that make them attractive candidates for lithium-battery applications.[1,2] Cation–anion combinations that exhibit negligible volatility coupled with high thermal and electrochemical stability, as well as a wide useable temperature range, result in intrinsically safer electrolytes.[3] To build safer devices, ILs have been widely explored as electrolyte components to combat the safety issues associated with conventional organic carbonate-based electrolytes.[4] However, hindered by their relatively higher viscosity, the electrochemical performance of IL-based cells is less competitive and, in fact, is generally assessed at a medium-to-high temperature and limited cycling rate.[5,6] In this paper, we present a strategy for the development of optimized ILs with improved fluidity by combining alkoxy-functionalized ammonium cations with asymmetric imide anions.

The substitution of an alkyl group with an alkoxy group in the cation structure is known to lower the lattice energy and improve the fluidity of the IL material.[7] The presence of the alkoxy function in the side chain modifies the Li–IL ion interactions within the electrolyte owing to the enhanced electron donicity and chelating ability of the cation, which consequently inhibits aggregation and improves bulk ionic conductivity.[8,9] Conversely, two anions have been extensively studied, bis(fluorosulfonyl)imide (FSI) and bis(trifluoromethanesulfonyl)imide (TFSI), which both have a rather symmetric structure. In general, FSI-based electrolytes have higher fluidity and conductivity, whereas TFSI-based electrolytes have higher thermal and electrochemical stability.[1] However, both FSI- and TFSI-based electrolytes tend to crystallize at low temperature or high salt concentration.[10,11] To overcome this drawback, we focus on the application of the (fluorosulfonyl)(trifluoromethanesulfonyl)imide (FTFSI) anion, which is the asymmetric imide anion with the lowest molecular weight. Furthermore, the melting point of LiFTFSI is also the lowest among the lithium salts with perfluoroalkylimide anions.[12] Previous studies have proven that the asymmetric FTFSI anion has a significant ability to lower the melting point or even totally prevent crystallization of RTILs.[13–15]

Herein, we report the synthesis of an IL composed of the *N*-*N*-diethyl-*N*-methyl-*N*-(2-methoxyethyl)ammonium (DEME) cation and the asymmetric FTFSI anion. DEME-ILs containing symmetric FSI and TFSI anions were also synthesized for comparison purposes. The physical, thermal, and electrochemical properties of these ILs were evaluated as such and upon lithium salt addition to assess their feasibility as electrolytes for lithium-battery applications. The preliminary battery tests confirmed the outstanding performance of FTFSI-based electrolytes in cells employing the high-voltage $Li_{1.2}Ni_{0.2}Mn_{0.6}O_2$ as the positive electrode and lithium metal as the negative electrode. Interestingly, the Li-concentrated FTFSI-based electrolyte outperformed the diluted one in terms of rate capability. To understand the concentration dependence of the effective Li-ion transport, a series of FTFSI-based electrolytes was prepared

[a] Dr. X. Gao, F. Wu, Dr. A. Mariani, Prof. Dr. S. Passerini
Helmholtz Institute Ulm (HIU)
Helmholtzstrasse 11, 89081 Ulm (Germany)
E-mail: stefano.passerini@kit.edu

[b] Dr. X. Gao, F. Wu, Dr. A. Mariani, Prof. Dr. S. Passerini
Karlsruhe Institute of Technology (KIT)
P.O. Box 3640, 76021 Karlsruhe (Germany)

Supporting Information and the ORCID identification number(s) for the author(s) of this article can be found under: https://doi.org/10.1002/cssc.201901739.

© 2019 Wiley-VCH Verlag GmbH & Co. KGaA, Weinheim

and investigated. The rather unexplored physical and transport properties of these electrolytes, such as viscosity, conductivity, and ionicity, along with ionic coordination of Li-ion speciation, are herein reported. To the best of our knowledge, only one study exists on the synthesis and characterization of DEMEFTFSI for lithium-battery applications,[16] but no detailed information on its transport properties and mechanisms is available.

Results and Discussion

A summary of the physicochemical characteristics of the neat ILs is presented in Figure 1. The densities and viscosities of the DEME-based ILs in the temperature range between 20 and 80 °C are plotted in Figure 1 a and b, respectively. The densities exhibit a typical decrease with rising temperature (linear trend) and decreasing anion size ($\rho^{DEMETFSI} > \rho^{DEMEFTFSI} > \rho^{DEMEFSI}$). In contrast, the viscosities exhibit an exponential decrease in the same temperature range. The lowest values were observed for DEMEFTFSI and, even more, DEMEFSI, owing to their smaller anion steric-hindrance effect.[17] Interestingly, benefitting from the asymmetric structure of FTFSI anion, the temperature dependence of DEMEFTFSI was more pronounced than that of DEMEFSI. When the temperature was increased from 20 to 80 °C, the viscosity of DEMEFTFSI decreased from 64.1 to 10.4 MPa s whereas that of DEMEFSI changed from 59.8 to 10.8 MPa s. Furthermore, the introduction of an ether function on the cation improves chain flexibility and lowers the viscosity.[15] Indeed, the viscosity of DEMETFSI (95.9 MPa s at 20 °C) was almost half that of the alkyl-ammonium analogue (N_{1224}TFSI, 160.7 MPa s at 20 °C),[18] resulting from the improved fluidity induced by the flexible ether function.

The thermal behavior of the DEME-based ILs was investigated by using differential scanning calorimetry (DSC), which indicated no crystallization or melting. Only a glass transition (T_g) was observed, as shown in Figure 1 c. Similar to the viscosity trend, the T_g of the three ILs was primarily determined by the strength of ion interactions,[19] with the lowest values observed in the cases of DEMEFSI and DEMEFTFSI. The above reported physicochemical properties, in terms of density, viscosity, and T_g, clearly indicated that a suitable combination of highly asymmetric anions and ether-functionalized cations can effectively lower the lattice energy and improve the fluidity of the resulting ILs. The key safety advantage of ILs arises from their low volatility and high thermal stability, resulting in low flammability.[20] Thermogravimetric analysis (TGA) measurements under a N_2 atmosphere (Figure 1 d) indicated that weight

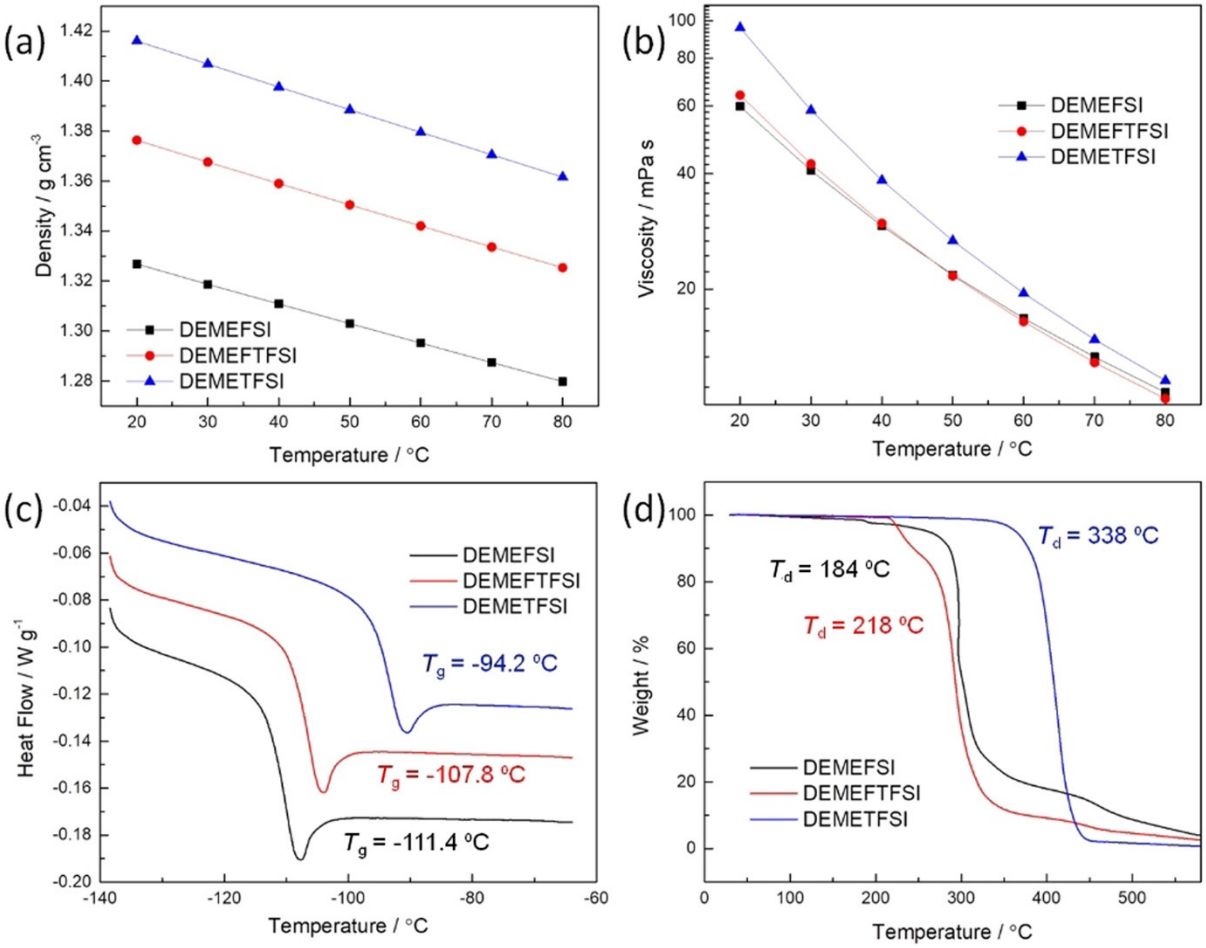

Figure 1. Dependence of (a) density and (b) dynamic viscosity on temperature for the DEME-based ILs. (c) DSC heating traces of DEME-based ILs. The traces are vertically shifted for clarity. (d) TGA curves for DEME-based ILs under a nitrogen atmosphere at a 10 °C min^{-1} heating rate.

© 2019 Wiley-VCH Verlag GmbH & Co. KGaA, Weinheim

losses only occurred at very high temperatures, confirming the low volatility, if any, of the ILs in the typical operative range of Li-metal batteries. However, thermal decompositions of the ionic species eventually occurred. Because of the lower stability of the F–S bond than that of the C–S and C–F bonds, DEMEFSI (onset $T_d = 184\,^{\circ}C$) and DEMEFTFSI (onset $T_d = 218\,^{\circ}C$) exhibited a lower decomposition temperature than DEMETFSI ($T_d = 338\,^{\circ}C$).[14] These values were inferior to those of the corresponding alkyl-ammonium analogues, but still far superior to any conventional organic-solvent-based electrolyte.[21,22]

To determine the compatibility of the studied ILs against lithium metal, stripping/plating galvanostatic cycles were performed by using symmetric Li/Li cells at 20 °C. The three ILs, DEMEFSI, DEMEFTFSI, and DEMETFSI, were added to LiFSI, LiFTFSI, and LiTFSI, respectively, to specifically investigate the effect of the anion on the electrochemical performance. For these specific tests, the lithium-salt content was set to 20 mol %. The shape of the stripping and plating curves was symmetrical for all three electrolytes, as shown in Figure 2a. In the initial cycles, the cells employing $DEMEFSI_{0.8}LiFSI_{0.2}$ (blue), $DEMEFTFSI_{0.8}LiFTFSI_{0.2}$ (red), and $DEMETFSI_{0.8}LiTFSI_{0.2}$ (black) electrolytes showed overpotentials of approximately 5, 7, and 20 mV, respectively, which were consistent with the conductivity of these electrolytes (Figure S1 in the Supporting Information). However, the overvoltage of the cell using $DEMEFSI_{0.8}LiFSI_{0.2}$ increased up to 10 mV after 100 cycles, whereas the overpotential of the $DEMEFTFSI_{0.8}LiFTFSI_{0.2}$ cell remained stable during the test. Electrochemical impedance spectroscopy (EIS) measurements were conducted on all cells along with the lithium stripping/plating tests. All spectra show a slightly depressed semicircle followed by a second feature at low frequencies, not always clearly visible, associated with the Li-ion diffusion in the electrolytes as well as in the solid–electrolyte interphase (SEI). The high-frequency intercept presents the electrolyte ionic resistance (R_{el}) whereas the second intercept in the low-frequency region refers to the electrolyte/electrode interfacial resistance (R_{int}), which includes the charge-transfer and passive-layer resistances.[23] The R_{el} values obtained from the Nyquist curves were approximately 6 Ω for $DEMEFSI_{0.8}LiFSI_{0.2}$, 10 Ω for $DEMEFTFSI_{0.8}LiFTFSI_{0.2}$, and 25 Ω for $DEMETFSI_{0.8}LiTFSI_{0.2}$. The R_{el} of each cell was practically unaffected by the repeated stripping/plating cycles, whereas the R_{int} values (considering the lowest frequency data) of the cells displayed different trends upon cycling. Changes in the impendence spectra are usually associated with the reconstruction of the native passive layer present on Li metal foil (SEI) caused by the lithium stripping and plating processes.[24] Therefore, it is interesting that the R_{int} of the cell using $DEMEFTFSI_{0.8}LiFTFSI_{0.2}$ electrolyte after 100 cycles (≈95 Ω) was even lower than that measured for the pristine cell (≈106 Ω). In contrast, the R_{int} values of the cells using FSI- and TFSI-based electrolytes increased from approximately 91 and 228 Ω to approximately 171 and 234 Ω, respectively. These results clearly demonstrate the outstanding compatibility of FTFSI-based electrolytes against lithium metal, which exhibited the lowest and the most stable interfacial resistance.

In addition to the promising thermal stability, another notable feature of IL-based electrolytes is their large electrochemical stability window.[4] To demonstrate the feasibility of DEME-based ILs as electrolytes in lithium batteries, high-voltage, lithium- and manganese-rich $Li_{1.2}Ni_{0.2}Mn_{0.6}O_2$ (LMR) was selected as the positive electrode material. The activation voltage of the LMR material is above 4.7 V, which is beyond the electrochemical stability range of most organic electrolytes employed in the state-of-the-art lithium-ion batteries.[25,26] Electrode potentials exceeding 4.5 V (vs. Li^+/Li) are known to cause oxidation of

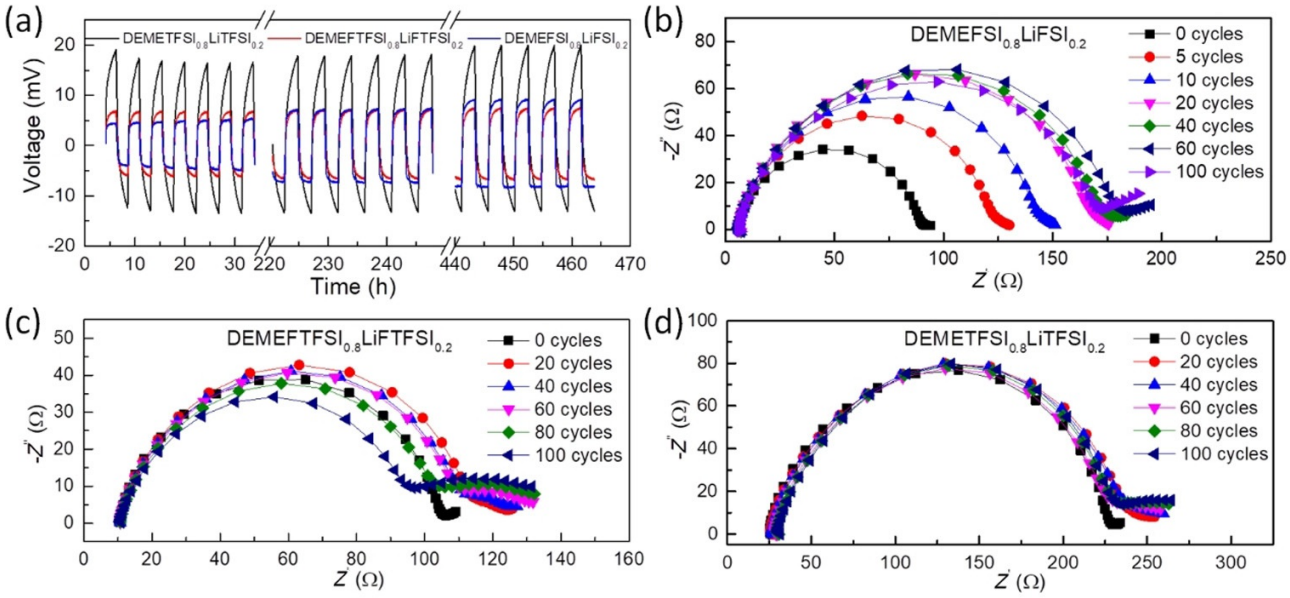

Figure 2. (a) Voltage versus time plot recorded upon stripping/plating cycling at a current of 0.025 mA cm^{-2} and a stripping–plating time of 2 h. Electrochemical impedance spectra of symmetrical Li/Li cells with (b) $DEMEFSI_{0.8}LiFSI_{0.2}$, (c) $DEMEFTFSI_{0.8}LiFTFSI_{0.2}$, and (d) $DEMETFSI_{0.8}LiTFSI_{0.2}$ electrolytes recorded during the stripping/plating cycle test. All measurements were performed at 20 °C.

© 2019 Wiley-VCH Verlag GmbH & Co. KGaA, Weinheim

the alkyl carbonates, which leads to rapid degradation of cell performance.[27] The anodic stability of the neat ILs and Li-containing (20 mol%) electrolytes considered in this work is always above 5 V (even considering the threshold at 0.01 mA cm^{-2}) with the anodic stability of DEMEFTFSI$_{0.8}$LiFTFSI$_{0.2}$ electrolyte slightly higher than that of DEMEFSI$_{0.8}$LiFSI$_{0.2}$ (Figure S2 in the Supporting Information). Concerning the cathodic stability, a few features were observed below 1.5 V for DEME-based ILs, which are probably related to the reduction of the ether-functionalized cation.[28] However, the reduction stability is effectively improved by the addition of the lithium salt, making these IL-based electrolytes suitable for application in high-voltage batteries.

The feasibility of the IL-based electrolytes for lithium batteries was further evaluated by galvanostatic cycling at 20 °C of the Li/LMR cells (Figure 3a) employing DEMETFSI$_{0.8}$LiTFSI$_{0.2}$ (blue), DEMEFTFSI$_{0.8}$LiFTFSI$_{0.2}$ (red), and DEMEFSI$_{0.8}$LiFSI$_{0.2}$ (black) electrolytes. After two activation cycles between 2.5 and 4.8 V, all cells were continuously cycled in the 2.5–4.6 V voltage range at C/2. The cell with the TFSI-based electrolyte delivered a meager capacity of approximately 65 mAh g^{-1}. This poor cell performance was ascribed to the low conductivity of the TFSI-based electrolyte (see Figure S1 in the Supporting Information), which consequently leads to high polarization.[29] As expected, the cells employing low-viscosity FTFSI- and FSI-based electrolytes delivered much higher initial capacities of approximately 150 and 160 mAh g^{-1}, respectively. However, the cell with the FSI-based electrolyte showed poor cycling stability (coulombic efficiency of ≈90%), and the capacity fading tended to progressively increase upon cycling. In contrast, the cell with FTFSI-based electrolyte had a coulombic efficiency approaching 99.8% and retained 96% of its initial capacity after 50 charge/discharge cycles, suggesting good stability of the electrolyte as well as both electrode/electrolyte interfaces. Based on the promising overall performance, cells employing the FTFSI-based electrolyte were subjected to long-term cycling. As shown in Figure 3b, the Li/DEMEFTFSI$_{0.8}$LiFTFSI$_{0.2}$/LMR cell delivered an initial capacity of 153 mAh g^{-1} within the voltage range of 2.5–4.6 V, with a capacity retention of 65.5% after 500 cycles and stable coulombic efficiencies exceeding 99.5%. The selected voltage profiles in Figure 3c show clear voltage fading upon cycling, which is probably owing to the gradual phase transformation of the positive electrode from a layered to a spinel morphology.[30]

As with any electrolyte systems, IL-based electrolytes also have their drawbacks. Their relatively high viscosity and, thus, lower conductivity limits the rate capabilities of IL-based cells. Conventional strategies propose mixing the ILs with organic solvents[28] or increasing the cell operating temperature[31] to mitigate this problem. However, it is not clear whether viscosity and conductivity are the only parameters restricting rate performance. Recently, several studies have proven that concentrated electrolytes based on organic solvents[32] or ILs[33–35] exhibit improved rate capabilities compared with those of diluted electrolytes. In an effort to understand the difference in performance of cells containing concentrated and dilute electrolytes, particularly in terms of the seemingly counterintuitive faster lithium transport mechanism at high concentration, a series of FTFSI-based electrolyte with different concentrations was prepared and examined. At room temperature, DEMEFTFSI$_{(1-x)}$LiFTFSI$_x$ mixtures up to a Li$^+$/DEME$^+$ ratio of 3:2 (60 mol% LiFTFSI) were all liquid, whereas the FSI- and TFSI-based electrolytes tend to form crystalline complexes at Li$^+$/DEME$^+$ ratios above 2:1.[10,11]

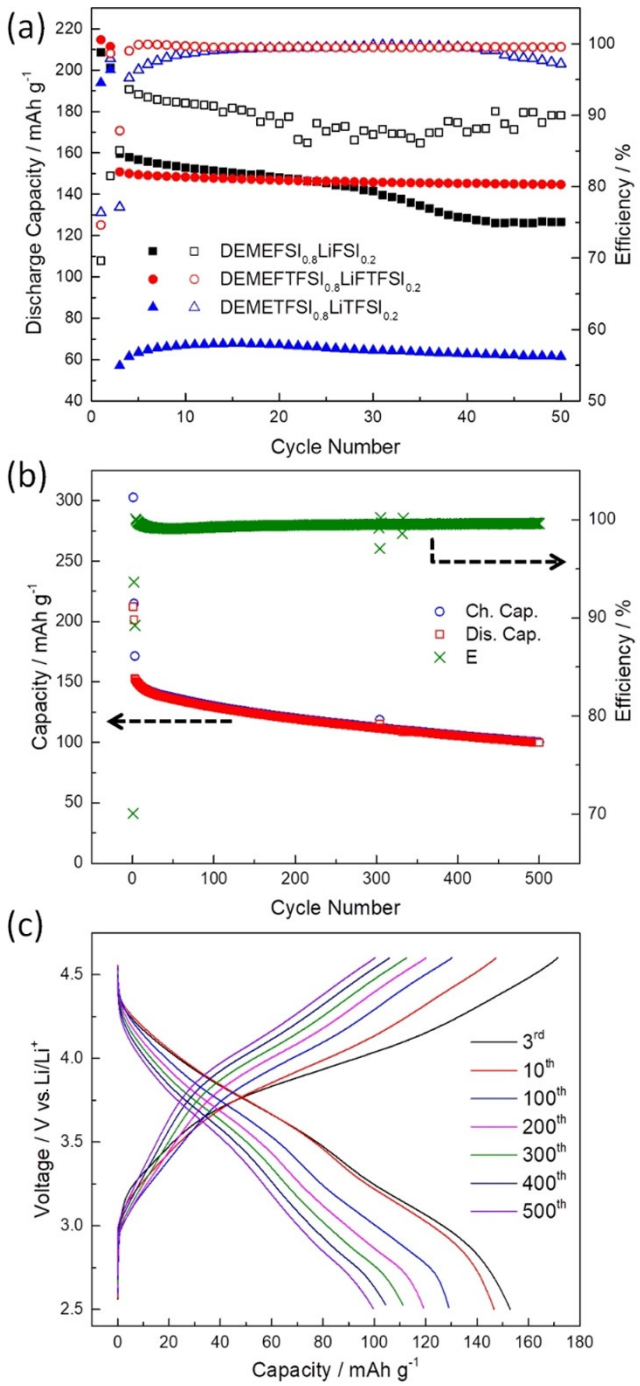

Figure 3. (a) Comparison of the discharge capacity (solid symbol) and coulombic efficiency (open symbol) of the Li/LMR cells (Swagelock-type) using different electrolytes. (b) Long-term cycling performance and (c) selected voltage profiles of a Li/DEMEFTFSI$_{0.8}$LiFTFSI$_{0.2}$/LMR pouch cell. All cells were cycled at C/2 in the voltage range of 2.5–4.6 V (from the third cycle) at 20 °C.

© 2019 Wiley-VCH Verlag GmbH & Co. KGaA, Weinheim

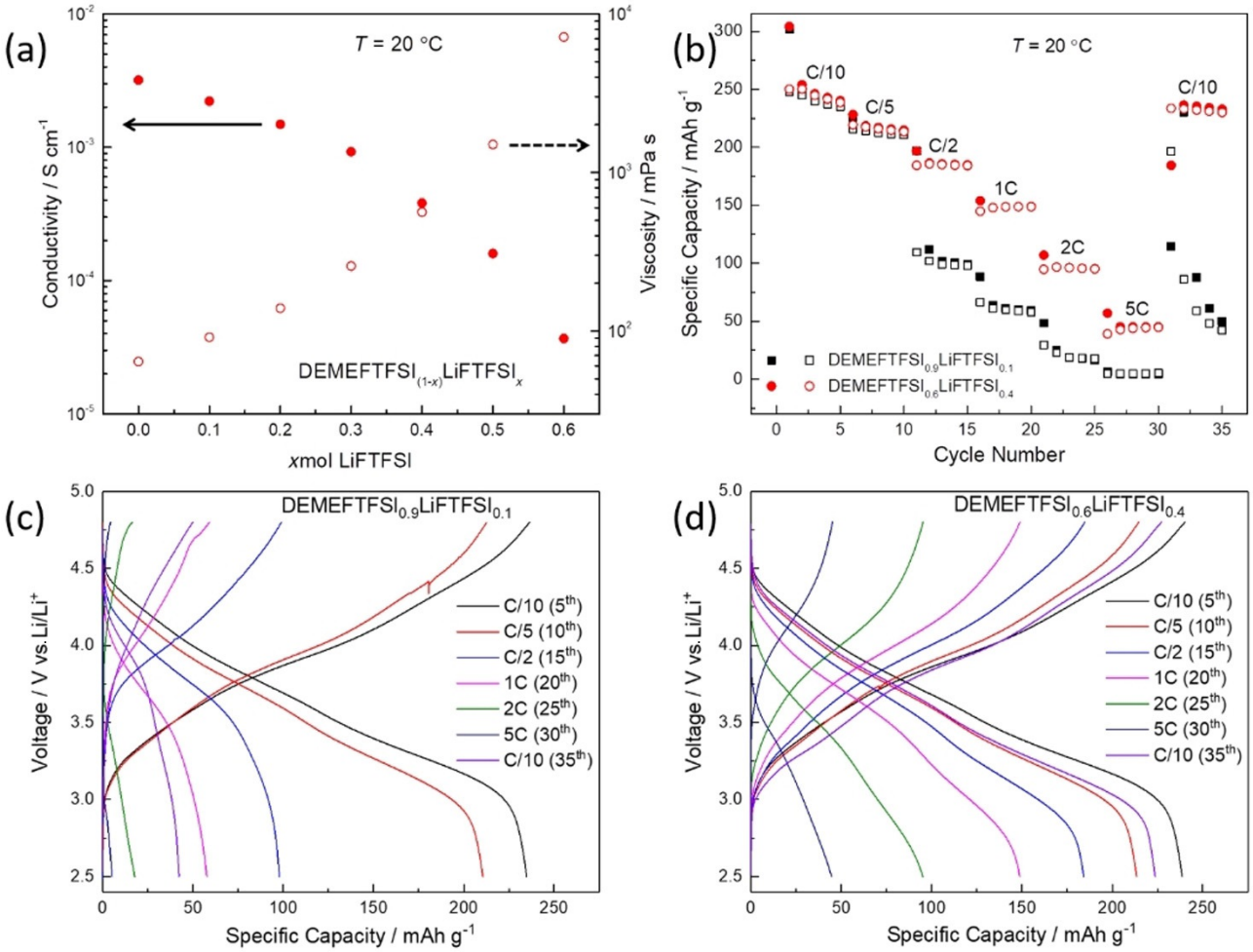

Figure 4. (a) Isothermal conductivity and viscosity of DEMEFTFSI$_{(1-x)}$LiFTFSI$_x$. (b) Rate performance in the voltage range of 2.5–4.8 V and selected voltage profiles of Li/DEMEFTFSI$_{(1-x)}$LiFTFSI$_x$/LMR cells with $x = 0.1$ (c) and 0.4 (d).

The concentration dependence of both the dynamic viscosity and bulk conductivity at 20 °C are shown in Figure 4a. Specifically, when the salt concentration increased from 10 to 40 mol%, the bulk conductivity decreased from 2.22 to 0.38 mS cm^{-1} whereas the dynamic viscosity increased from 91.6 to 562.3 MPa s. A comparison of the rate performance of the 10 and 40 mol% electrolytes in the Li/LMR cells is shown in Figure 4b. The tests were performed by using the cutoff limits of 2.5 and 4.8 V at 20 °C. In this voltage range, both cells delivered an initial capacity of approximately 250 mAh g^{-1}. The performance of both cells was comparable after 10 cycles at C/10 and C/5. Interestingly, when the C-rate was further increased to C/2 and 1C, the capacity of the cell with the diluted electrolyte decreased abruptly to less than 100 mAh g^{-1} whereas the capacity of the cell with the concentrated electrolyte stabilized at approximately 185 and 148 mAh g^{-1} at C/2 and 1C, respectively. This performance was very unexpected based on the substantially lower conductivity and higher viscosity of the concentrated electrolyte with respect to the diluted one. Additionally, the cell employing DEMEFTFSI$_{0.6}$LiFTFSI$_{0.4}$ as the electrolyte fully recovered its capacity when the C-rate was brought back to C/10. In contrast, the cell employing DEMEFTFSI$_{0.9}$LiFTFSI$_{0.1}$ delivered an extremely low capacity at 5 C, which was probably owing to the lower diffusion limiting current density.[36,37] The selected voltage profiles of the cells employing the 10 and 40 mol% electrolytes are presented in Figure 4c and d, respectively. The cell polarization of the concentrated electrolyte increased gradually with the cycling rate whereas an abrupt polarization increase was observed for the diluted electrolyte above C/2.

The above-reported results clearly demonstrated that knowing the dynamic viscosity and bulk conductivity of the electrolyte is not sufficient to predict the rate performance of the cell. Further studies about the concentrated electrolytes in terms of ionicity, ionic coordination, and Li-ion speciation are needed to better understand the ion transport mechanism. The conductivity and viscosity of the DEMEFTFSI$_{(1-x)}$LiFTFSI$_x$ electrolytes, measured in the temperature range between 0 and 80 °C, are shown in Figure 5a and b, respectively. Upon increasing Li^+ ion content, the dynamic viscosity increased whereas the bulk conductivity concurrently decreased, both following the typical Vogel–Tammann–Fulcher (VTF) behavior often reported for IL-based electrolytes.[31] The trends of bulk conductivity and dynamic viscosity are described by the VTF Equations (1) and (2),

© 2019 Wiley-VCH Verlag GmbH & Co. KGaA, Weinheim

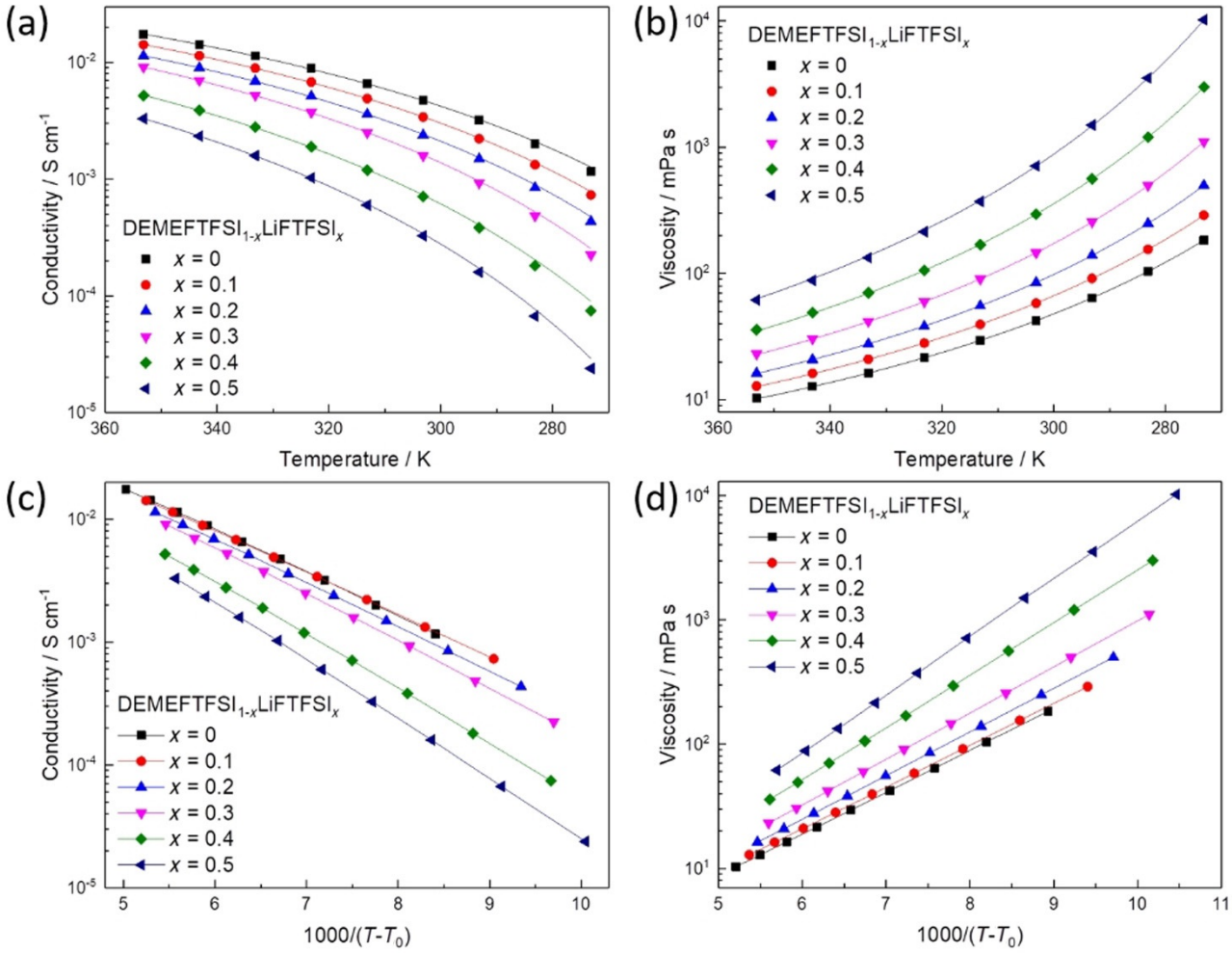

Figure 5. (a) Conductivity and (b) viscosity of DEMEFTFSI$_{(1-x)}$LiFTFSI$_x$ mixtures. The symbols correspond to experimental data whereas the lines represent the VTF fit of the experimental data. Corresponding VTF plots of (c) conductivity and (d) viscosity reported versus 1000/($T-T_0$), respectively.

respectively:

$$\sigma(T) = \sigma_\infty exp\left(-\frac{E_a}{k_B(T-T_0)}\right) \quad (1)$$

$$\eta(T) = \eta_\infty exp\left(-\frac{E_a}{k_B(T-T_0)}\right) \quad (2)$$

in which E_a [eV] is the activation energy, k_B (8.62×10^{-5} eV K^{-1}) is the Boltzmann constant, T [K] is the absolute temperature, T_0 [K] is the correction parameter correlated to T_g, and σ_∞ and η_∞ are the ionic conductivity and viscosity at infinite temperature, respectively. The fit results are plotted in Figure 6a, b, and the fit parameters are reported in Table 1. The activation energy estimated from bulk conductivity of neat DEMEFTFSI coincided with that derived for the dynamic viscosity (2.91×10^{-2} eV). Such an excellent agreement suggests that ion conduction within the neat ILs is dominated by viscosity. The two activation energy values remained in good agreement with increasing LiFTFSI concentration, although the activation energy from the dynamic viscosity was slightly higher than that from con-

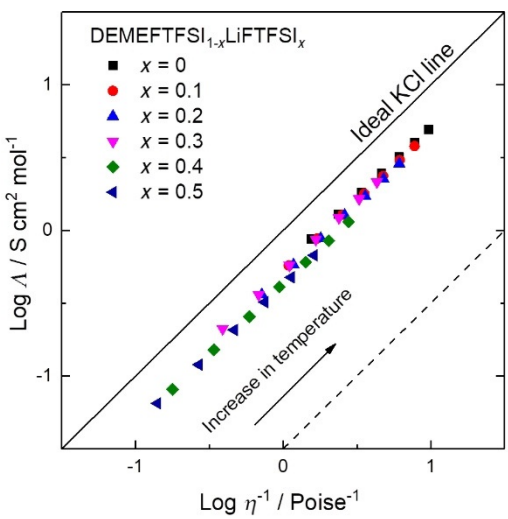

Figure 6. Walden plot showing relationships between inverse viscosity and molar conductivity for DEMEFTFSI$_{(1-x)}$LiFTFSI$_x$ mixtures (temperature range 20–80 °C; 1 Poise = 100 MPa s).

© 2019 Wiley-VCH Verlag GmbH & Co. KGaA, Weinheim

Table 1. T_g obtained from DSC and VTF fit parameters of DEMEFTFSI$_{(1-x)}$LiFTFSI$_x$ mixtures obtained from viscosity and ionic conductivity.

x LiFTFSI [mol]	T_g [K]	Conductivity E_a [$\times 10^{-2}$ eV]	T_0 [K]	Viscosity E_a [$\times 10^{-2}$ eV]	T_0 [K]
0	165.29	2.91	154.23	2.91	161.18
0.1	170.05	2.86	162.59	2.90	166.81
0.2	176.19	2.98	166.13	3.02	170.18
0.3	185.89	3.17	170.06	3.20	174.52
0.4	194.21	3.61	169.75	3.65	174.93
0.5	201.98	3.96	173.62	3.99	177.59

ductivity. T_0 is often referred to as zero configurational entropy or the thermodynamic ideal glass-transition temperature.[17,29] The experimental T_g for the DEMEFTFSI$_{(1-x)}$LiFTFSI$_x$ mixtures were obtained from DSC measurements (Figure S3 in the Supporting Information) and are summarized in Table 1. In general, the T_0 values derived from the fit of conductivity and viscosity increased with salt concentration, which was in good agreement with the corresponding increasing trend of experimental T_g. By using the T_0 values derived from the fit results, typical linear trends of the logarithm of conductivity and viscosity versus $1000/(T-T_0)$ were obtained, as shown in Figure 5 c, d.

By using the Walden equation [Eq. (3)] described by Angell et al.,[38] the molar conductivity of DEMEFTFSI$_{(1-x)}$LiFTFSI$_x$ mixtures was plotted versus their inverse viscosity, as depicted in Figure 6.

$$\Lambda\eta^{\alpha} = C \tag{3}$$

in which η is the viscosity [Poise], α is an adjustable parameter, C is a temperature-dependent constant, and Λ is the molar conductivity [S cm^2 mol^{-1}]. The molar conductivity of the DEMEFTFSI$_{(1-x)}$LiFTFSI$_x$ mixtures was calculated by using the experimental density values reported in Figure S4 in the Supporting Information. Dilute aqueous KCl solutions are often used as a point of reference. They represent an "ideal" solution in which the ions are fully dissociated, that is, any ionic interaction can be neglected. The IL-based electrolytes fall below this ideal KCl solution trend line, indicating the existence of ionic interactions impeding independent ion motions in the liquid. This is particularly effective when ions tend to associate into a neutral ion-pair, which does not contribute to the bulk conductivity at all. Therefore, deviations from the Walden rule are taken as an effective, although qualitative, method to characterize the ionicity of IL-based electrolytes.[39] With regards to the electrolytes investigated in this study, all plots were close together with little sign of strong ion association. Additionally, their slopes (see Figure 6) were between 0.95 and 0.97, that is, in the range generally observed for other IL-based electrolytes.[10,38,40] The C value, which represents the distance from the "ideal" aqueous KCl line ($\alpha=1$, $C=0$), changed from -0.24 for the neat IL to -0.37 for the 50 mol% LiFTFSI electrolyte. Although the ionicity decreased with increasing LiFTFSI concentration, the progressive addition of LiFTFSI into the IL did not seem to have a large effect on the degree of ion association.[39]

In an effort to understand the ionic coordination of Li-ion speciation, Raman spectroscopy was employed to assess the interactions between Li^+ and $FTFSI^-$ in the electrolytes as a function of the lithium salt concentration. Similar to TFSI- or FSI-based ILs, FTFSI-based ILs exhibit the characteristic imide expansion–contraction (exp–con) mode in the spectral region between 700 and 800 cm^{-1}, which is sensitive to both the anion conformation and coordination.[41] The Raman spectra of DEMEFTFSI$_{(1-x)}$LiFTFSI$_x$ mixtures in the spectral region between 700 and 800 cm^{-1} are shown in Figure 7. For the neat IL, the

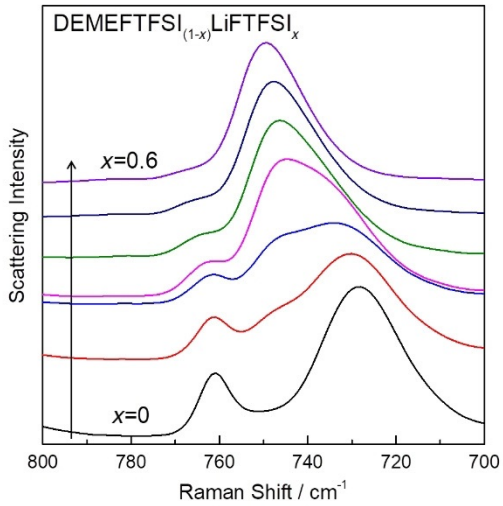

Figure 7. Raman spectra of DEMEFTFSI$_{(1-x)}$LiFTFSI$_x$ mixtures in the characteristic FTFSI expansion–contraction mode region. The spectra are normalized and vertically shifted for clarity.

broad peak centered at 729 cm^{-1} was attributed to vibrations of "free" $FTFSI^-$ anions whereas the peak centered at 762 cm^{-1} was associated with the mixed vibrational mode of CF_3 deformation and SF stretching.[42] The progressive addition of LiFTFSI into the IL gave rise to a shoulder that evolved into a distinct peak centered at 747 cm^{-1}, which was clearly related to the Li^+–$FTFSI^-$ coordination. As the concentration of LiFTFSI in DEMEFTFSI$_{(1-x)}$LiFTFSI$_x$ increased, the intensity of the 747 cm^{-1} peak increased. Finally, the peak shifted to 751 cm^{-1} at the highest LiFTFSI concentration. Concurrently, the intensities of both the lower-frequency component (729 cm^{-1}) and the higher-frequency component (762 cm^{-1}) decreased. Previous studies[41,43] have shown that as the salt concentration increases, the ionic coordination of Li-ion speciation becomes complex. The ratio of contact ion-pairs and, especially, aggregates increases whereas the number of "free" $FTFSI^-$ anions drastically decreases.

Two types of Li-ion speciation can be identified at LiFTFSI concentrations above and below 30 mol%. Below 30 mol%, the two peaks correspond to the coexistence of "free" $FTFSI^-$ anions (729 cm^{-1}) and Li^+-coordinated $FTFSI^-$ anions (747 cm^{-1}). The Li-ion species are primarily small complexes, and thus the Li^+ transport is mostly derived from the diffusion-controlled vehicular transport mechanism.[44] At 40 mol%

© 2019 Wiley-VCH Verlag GmbH & Co. KGaA, Weinheim

LiFTFSI and above, the coordinated $FTFSI^-$ peak further shifts to 751 cm^{-1} whereas the "free" $FTFSI^-$ peak almost vanishes. According to previous studies, the feature at 751 cm^{-1} can be assigned to the $FTFSI^-$ anions involved in aggregate species because above this concentration the $FTFSI^-/Li^+$ ratio is 2.5:1 or lower.[45] The formation of such aggregates results in an increased size and decreased mobility of the charge-carrying species, as evidenced by the increased dynamic viscosity and lowered bulk conductivity with increasing LiFTFSI content. However, the formation of aggregate species seems to have a rather different influence on the transport of Li^+ ions. It has been proposed that, in a concentrated electrolyte, the Li^+ transport mechanism changes from a diffusion-controlled vehicular transport of small Li^+ complexes to hopping-type ion transport through the exchange of anions in the Li^+-containing aggregate species.[37,46–50] This must be true to explain the exceptional performance of the Li/LMR cell employing the DEMEFTFSI$_{0.6}$LiFTFSI$_{0.4}$ at high rates, despite its substantially lower conductivity and higher viscosity than the electrolytes containing 10 and 20 mol% LiFTSFI.

Conclusions

Three *N*-*N*-diethyl-*N*-methyl-*N*-(2-methoxyethyl)ammonium (DEME)-based ionic liquids (ILs) with various imide anions were successfully prepared and characterized. Physicochemical characterization indicated that the combination of the alkoxy function in $DEME^+$ together with the (fluorosulfonyl)(trifluoromethanesulfonyl)imide ($FTFSI^-$) asymmetry successfully lowers the lattice energy, resulting in improved fluidity of DEMEFTFSI. Upon the addition of lithium salt, the FTFSI-based electrolyte was tested in Li/$Li_{1.2}Ni_{0.2}Mn_{0.6}O_2$ cells, showing outstanding electrochemical performance even at room temperature. Moreover, preliminary battery tests demonstrated that the rate performance of cells containing electrolytes with a high Li concentration was significantly improved, confirming that the effective Li-ion transport is decoupled from the dynamic viscosity and bulk conductivity owing to the establishment of the hopping-type ion transport through the exchange of coordination ligands and Li^+-containing aggregate species.

Experimental Section

Electrolyte preparation and characterization

Lithium bis(trifluoromethanesulfonyl)imide (LiTFSI, 99.5%, 3 M), lithium (fluorosulfonyl)(trifluoromethanesulfonyl)imide (LiFTFSI, 98%, Provisco CS Ltd), lithium bis(fluorosulfonyl)imide (LiFSI, 98%, Provisco CS Ltd), *N*,*N*-diethylmethylamine (97%, Sigma Aldrich), and 2-bromoethyl methyl ether (95%, TCI) were used as received. Ultrapure water (Millipore) was used throughout the experiment. The DEMETFSI, DEMEFTFSI, and DEMEFSI ILs were prepared following the procedure described in the literature.[51] Briefly, the DEME-based ILs were synthesized according to a two-step synthesis procedure, involving the direct alkylation of *N*,*N*-diethylmethylamine with 2-bromoethyl methyl ether to form the bromide precursor, which was subjected to anion exchange with LiFSI, LiFTFSI, and LiTFSI in aqueous solution. The hydrophobic ILs were rinsed several times with deionized water to eliminate the water-soluble impurities, LiBr and excess Li salt. Then, the ILs were dried under vacuum for 2 days. The electrolyte solutions were prepared by mixing appropriate amounts of lithium salt and IL in an argon-filled glovebox (MBRAUN), with oxygen and water contents lower than 0.1 ppm. The ILs and electrolyte solutions were all dried under vacuum by using a turbomolecular pump (below 10^{-7} mbar). The water content of the ILs and electrolyte solutions was less than 5 ppm (detection limit) as determined by Karl-Fischer titration.

The density was measured with a density meter (Anton-Paar DMA 4100M). The viscosity measurements were performed by using a rheometer (Anton-Paar Physica MCR301) in the cone-plate geometry. Both the viscosity and the density measurements were performed inside a dry room. TGA measurements (Netzch) were performed up to 580 °C at 10 °C min^{-1} under N_2 atmosphere. DSC measurements were performed by using a differential scanning calorimeter (TA Instruments Q2000) with liquid N_2 cooling. The samples were hermetically sealed in aluminum pans in the glovebox. The thermal treatment included cycling from −140 to 100 °C at a rate of 5 °C min^{-1}. Conductivities were determined by a conductometer equipped with a frequency analyzer and a thermostatic bath (MMates Italia). The ILs were sealed in glass conductivity cells (mounted in the glovebox) equipped with two platinum-platinized electrodes. The cell constants were determined by using a 0.01 M KCl standard solution. The measurements were run in the temperature range from 0 to 80 °C, and the equilibration time at each temperature was 1 h. The Raman measurements were recorded on a combined Raman–FTIR spectrometer (RAM II FT-Raman module of Bruker Vertex70) equipped with a laser wavelength of 1064 nm and laser power of 300 mW. The collected spectra are the average of 500 scans at an optical resolution of 2 cm^{-1}.

Electrochemical characterization

The electrochemical stability windows (ESWs) of the neat ILs and the electrolyte solutions were determined by linear-sweep voltammetry (LSV) by using modified three electrode Swagelock cells at a scan rate of 1 mV s^{-1}. A platinum disk electrode (1 mm diameter) was used as working electrode, and Li metal (Honjo Metal, battery grade) was used for the reference and counter electrodes. The lithium stripping/plating tests were performed with symmetric Li/Li cells, in which a constant current density of 0.025 mA cm^{-2} was imposed and the cell polarization was reversed every 2 h. EIS measurements were also performed to monitor the change in the interfacial resistance during stripping/plating. The amplitude of the AC was 10 mV in the frequency range from 1 Hz to 200 kHz. The tests were conducted by using a VMP3 galvanostat/potentiostat (Bio-Logic), and the cells were maintained at 20 ± 2 °C in the climatic chamber.

The lithium- and manganese-rich cathode ($Li_{1.2}Ni_{0.2}Mn_{0.6}O_2$) was prepared according to the reported solid-state method.[52] The cathodes were composed of 85 wt% active material, 10 wt% SuperC65 (IMERYS) as conductive carbon, and 5 wt% polyvinylidene fluoride (Solef 6020) as binder. The average mass loading of active material was approximately 3 mg cm^{-2}. Three-electrode Swagelock cells were assembled in the argon-filled glovebox with water and oxygen content below 0.1 ppm. Whatman GF/D glass-fiber separators were soaked with the electrolyte, and Li metal was used as the counter and reference electrodes. Galvanostatic cycling was conducted by using a battery tester (Maccor, model 4300). All electrochemical tests were performed at 20 °C. The C-rate of 1C corresponds to an applied current of 250 mA g^{-1} or, for the electrodes' areal loading used, approximately 0.75 mA cm^{-2}.

© 2019 Wiley-VCH Verlag GmbH & Co. KGaA, Weinheim

Acknowledgements

X.G. acknowledges the financial support of the Sino-German Postdoc Scholarship Program (No.57343410). F.W. acknowledges the financial support from the Chinese Scholarship Council. All authors acknowledge the support of the Helmholtz Association. The authors thank Dr. Kim Guk-tae for the valuable suggestions.

Conflict of interest

The authors declare no conflict of interest.

Keywords: asymmetric anions · ether-functionalized cations · high concentrated electrolytes · ionic liquids · Li-rich cathode

[1] G. B. Appetecchi, M. Montanino, S. Passerini, *ACS Symp. Ser.* **2012**, *1117*, 67–128.
[2] D. R. MacFarlane, M. Forsyth, P. C. Howlett, M. Kar, S. Passerini, J. M. Pringle, H. Ohno, M. Watanabe, F. Yan, W. Zheng, S. Zhang, J. Zhang, *Nat. Rev. Mater.* **2016**, *1*, 15005.
[3] M. Watanabe, M. L. Thomas, S. Zhang, K. Ueno, T. Yasuda, K. Dokko, *Chem. Rev.* **2017**, *117*, 7190–7239.
[4] A. Lewandowski, A. Świderska-Mocek, *J. Power Sources* **2009**, *194*, 601–609.
[5] A. Moretti, S. Jeong, G. A. Giffin, S. Jeremias, S. Passerini, *J. Power Sources* **2014**, *269*, 645–650.
[6] M. Moreno, E. Simonetti, G. B. Appetecchi, M. Carewska, M. Montanino, G.-T. Kim, N. Loeffler, S. Passerini, *J. Electrochem. Soc.* **2017**, *164*, A6026–A6031.
[7] S. Tang, G. A. Baker, H. Zhao, *Chem. Soc. Rev.* **2012**, *41*, 4030–4066.
[8] M. Kunze, E. Paillard, S. Jeong, G. B. Appetecchi, M. Schoönhoff, M. Winter, S. Passerini, *J. Phys. Chem. C* **2011**, *115*, 19431–19436.
[9] J. Von Zamory, G. A. Giffin, S. Jeremias, F. Castiglione, A. Mele, E. Paillard, S. Passerini, *Phys. Chem. Chem. Phys.* **2016**, *18*, 21539–21547.
[10] H. Yoon, A. S. Best, M. Forsyth, D. R. MacFarlane, P. C. Howlett, *Phys. Chem. Chem. Phys.* **2015**, *17*, 4656–4663.
[11] W. A. Henderson, S. Passerini, *Chem. Mater.* **2004**, *16*, 2881–2885.
[12] K. Kubota, T. Nohira, R. Hagiwara, H. Matsumoto, *Chem. Lett.* **2010**, *39*, 1303–1304.
[13] S. Jeremias, M. Carewska, L. Conte, S. Passerini, G. B. Appetecchi, *RSC Adv.* **2013**, *3*, 17755–17761.
[14] J. Reiter, S. Jeremias, E. Paillard, M. Winter, S. Passerini, *Phys. Chem. Chem. Phys.* **2013**, *15*, 2565–2571.
[15] J. Reiter, E. Paillard, L. Grande, M. Winter, S. Passerini, *Electrochim. Acta* **2013**, *91*, 101–107.
[16] H. Matsumoto, N. Terasawa, S. Tsuzuki, H. Sakaebe, *ECS Trans.* **2011**, *33*, 37–42.
[17] S. Jeong, S. Li, G. B. Appetecchi, S. Passerini, *Energy Storage Mater.* **2019**, *18*, 1–9.
[18] M. L. P. Le, N. A. Tran, H. P. K. Ngo, T. G. Nguyen, V. M. Tran, *J. Solution Chem.* **2015**, *44*, 2332–2343.
[19] F. Makhlooghiazad, J. Guazzagaloppa, L. A. O'Dell, R. Yunis, A. Basile, P. C. Howlett, M. Forsyth, *Phys. Chem. Chem. Phys.* **2018**, *20*, 4721–4731.
[20] G. G. Eshetu, S. Jeong, P. Pandard, A. Lecocq, G. Marlair, S. Passerini, *ChemSusChem* **2017**, *10*, 3146–3159.
[21] C. Arbizzani, G. Gabrielli, M. Mastragostino, *J. Power Sources* **2011**, *196*, 4801–4805.
[22] C. L. Campion, W. Li, B. L. Lucht, *J. Electrochem. Soc.* **2005**, *152*, A2327.
[23] J. R. Macdonald, *J. Electroanal. Chem.* **1987**, *223*, 25–50.
[24] A. Basile, A. F. Hollenkamp, A. I. Bhatt, A. P. O'Mullane, *Electrochem. Commun.* **2013**, *27*, 69–72.
[25] J. Zheng, S. Myeong, W. Cho, P. Yan, J. Xiao, C. Wang, J. Cho, J. G. Zhang, *Adv. Energy Mater.* **2017**, *7*, 1601284.
[26] L. Sun, X. Yi, C. Shi, X. Ren, Y. Gao, Y. Li, P. Zhang, *Int. J. Electrochem. Sci.* **2017**, *12*, 4756–4767.
[27] A. D. Robertson, P. G. Bruce, *Chem. Mater.* **2003**, *15*, 1984–1992.
[28] M. A. Navarra, K. Fujimura, M. Sgambetterra, A. Tsurumaki, S. Panero, N. Nakamura, H. Ohno, B. Scrosati, *ChemSusChem* **2017**, *10*, 2496–2504.
[29] G. A. Elia, U. Ulissi, F. Mueller, J. Reiter, N. Tsiouvaras, Y. K. Sun, B. Scrosati, S. Passerini, J. Hassoun, *Chem. Eur. J.* **2016**, *22*, 6808–6814.
[30] J. Zheng, J. Xiao, M. Gu, P. Zuo, C. Wang, J. G. Zhang, *J. Power Sources* **2014**, *250*, 313–318.
[31] G. A. Elia, U. Ulissi, S. Jeong, S. Passerini, J. Hassoun, *Energy Environ. Sci.* **2016**, *9*, 3210–3220.
[32] Y. Yamada, J. Wang, S. Ko, E. Watanabe, A. Yamada, *Nat. Energy* **2019**, *4*, 269–280.
[33] H. Yoon, P. C. Howlett, A. S. Best, M. Forsyth, D. R. MacFarlane, *J. Electrochem. Soc.* **2013**, *160*, A1629–A1637.
[34] G. A. Giffin, A. Moretti, S. Jeong, S. Passerini, *J. Power Sources* **2017**, *342*, 335–341.
[35] M. J. Marczewski, B. Stanje, I. Hanzu, M. Wilkening, P. Johansson, *Phys. Chem. Chem. Phys.* **2014**, *16*, 12341–12349.
[36] K. Yoshida, M. Tsuchiya, N. Tachikawa, K. Dokko, M. Watanabe, *J. Electrochem. Soc.* **2012**, *159*, A1005–A1012.
[37] K. Dokko, D. Watanabe, Y. Ugata, M. L. Thomas, S. Tsuzuki, W. Shinoda, K. Hashimoto, K. Ueno, Y. Umebayashi, M. Watanabe, *J. Phys. Chem. B* **2018**, *122*, 10736–10745.
[38] C. A. Angell, N. Byrne, J. P. Belieres, *Acc. Chem. Res.* **2007**, *40*, 1228–1236.
[39] G. M. A. Girard, M. Hilder, H. Zhu, D. Nucciarone, K. Whitbread, S. Zavorine, M. Moser, M. Forsyth, D. R. MacFarlane, P. C. Howlett, *Phys. Chem. Chem. Phys.* **2015**, *17*, 8706–8713.
[40] W. Xu, E. I. Cooper, C. A. Angell, *J. Phys. Chem. B* **2003**, *107*, 6170–6178.
[41] G. A. Giffin, A. Moretti, S. Jeong, K. Pilar, M. Brinkkötter, S. G. Greenbaum, M. Schönhoff, S. Passerini, *ChemSusChem* **2018**, *11*, 1981–1989.
[42] G. A. Giffin, N. Laszczynski, S. Jeong, S. Jeremias, S. Passerini, *J. Phys. Chem. C* **2013**, *117*, 24206–24212.
[43] M. Brinkkötter, G. A. Giffin, A. Moretti, S. Jeong, S. Passerini, M. Schönhoff, *Chem. Commun.* **2018**, *54*, 4278–4281.
[44] J. B. Haskins, W. R. Bennett, J. J. Wu, D. M. Hernández, O. Borodin, J. D. Monk, C. W. Bauschlicher, J. W. Lawson, *J. Phys. Chem. B* **2014**, *118*, 11295–11309.
[45] J. C. Lassègues, J. Grondin, C. Aupetit, P. Johansson, *J. Phys. Chem. A* **2009**, *113*, 305–314.
[46] Y. Ugata, M. L. Thomas, T. Mandai, K. Ueno, K. Dokko, M. Watanabe, *Phys. Chem. Chem. Phys.* **2019**, *21*, 9759–9768.
[47] C. J. F. Solano, S. Jeremias, E. Paillard, D. Beljonne, R. Lazzaroni, *J. Chem. Phys.* **2013**, *139*, 034502.
[48] M. Forsyth, H. Yoon, F. Chen, H. Zhu, D. R. MacFarlane, M. Armand, P. C. Howlett, *J. Phys. Chem. C* **2016**, *120*, 4276–4286.
[49] F. Chen, M. Forsyth, *Phys. Chem. Chem. Phys.* **2016**, *18*, 19336–19344.
[50] A. Nakanishi, K. Ueno, D. Watanabe, Y. Ugata, Y. Matsumae, J. Liu, M. L. Thomas, K. Dokko, M. Watanabe, *J. Phys. Chem. C* **2019**, *123*, 14229–14238.
[51] X. Gao, A. Mariani, S. Jeong, X. Liu, X. Dou, M. Ding, A. Moretti, S. Passerini, *J. Power Sources* **2019**, *423*, 52–59.
[52] J. Li, R. Klöpsch, M. C. Stan, S. Nowak, M. Kunze, M. Winter, S. Passerini, *J. Power Sources* **2011**, *196*, 4821–4825.

Manuscript received: June 27, 2019
Revised manuscript received: July 18, 2019
Accepted manuscript online: July 19, 2019
Version of record online: August 13, 2019

© 2019 Wiley-VCH Verlag GmbH & Co. KGaA, Weinheim